Oxygen-vacancy-induced memory effect and large recoverable strain in a barium titanate single crystal

Yihui Zhang,[1] Jiangyu Li,[1,2,*,†] and Daining Fang[1,3,*,‡]
[1]*AML, Department of Engineering Mechanics, Tsinghua University, Beijing 100084, China*
[2]*Department of Mechanical Engineering, University of Washington, Seattle, Washington 98195-2600, USA*
[3]*LTCS, College of Engineering, Peking University, Beijing 100871, China*
(Received 21 May 2010; revised manuscript received 25 June 2010; published 10 August 2010)

A phase field model is developed in this paper to study the influences of oxygen vacancies on domain evolutions under electric field in $BaTiO_3$ single crystal. The oxygen vacancies are modeled as defect dipoles, enabling the capture of domain memory effect. Three different domain structures are studied, and the distributions of defect density and the electromechanical responses under electric loading are simulated. The simulations reproduce well the reversible domain switching and large recoverable electric-field-induced strain observed in experiments on both engineered domain structure and single domain structure. It is also discovered that double hysteresis loop, stepwise hysteresis loop and shifted hysteresis loop can emerge due to vacancy induced depolarization field, which explains well the previous experimental observations. The results also indicate that domain memory effect and non-180° domain switching are the mechanisms for large recoverable electric-field-induced strain in ferroelectrics with oxygen vacancies.

DOI: 10.1103/PhysRevB.82.064103 PACS number(s): 77.80.Dj, 73.40.−c, 61.72.jd

I. INTRODUCTION

Oxygen vacancy, as a kind of common defects, widely exists in ferroelectrics. It can be created in different ways, such as nonstoichiometry, extrinsic doping,[1] etc. The extent of oxygen vacancies in ferroelectrics can be modulated by adopting different oxidation processes[2] and donor dopants[3] but cannot be completely eliminated. Therefore, oxygen vacancies have significant influences on the ferroelectric properties and it is important to understand the mechanisms of oxygen vacancies in influencing the electromechanical properties of ferroelectric materials.

Many experiments have been performed to investigate the roles of oxygen vacancies on different aspects of ferroelectric behaviors. On one hand, the presence of oxygen vacancies can lead to gradual degradation of ferroelectric properties in aged ferroelectric materials, resulting polarization fatigue.[4–8] On the other hand, the oxygen vacancy possesses a general symmetry-conforming property which can be effectively utilized to achieve large recoverable electric-field-induced strain.[9] Related experiments demonstrated that aged ferroelectric single crystal with an engineered domain configuration[9,10] or a single domain structure[11] can exhibit double hysteresis loop and large recoverable electrostrain. Similar aging behaviors have also been reported in Mn-doped alkaline niobate-based and lead zirconic titanate ferroelectrics that are composed of tetragonal, orthorhombic, and rhombohedral perovskite structures.[12]

Based on these experimental observations, some theoretical and numerical models have been developed to investigate the migrations and distributions of oxygen vacancies in ferroelectrics. The *ab initio* simulations were carried out to study the interactions of oxygen vacancies with both 180° and 90° domain walls, indicating a sudden electric potential decrease across the 90° domain wall.[13–15] Dawber and Scott[16] derived an analytic solution for polarization fatigue in a phenomenological framework, which yields good agreement with experimental data for lead zirconate titanate/Pt system, including the dependence of polarizations on different frequencies, different voltages, and different temperatures. Lo and co-workers[17,18] developed a random two-dimensional four-state Potts model to study the roles of oxygen vacancy in lead titanate zirconate ferroelectric thin film, including polarization fatigue behavior, and double hysteresis behavior. This model was established for ceramics and did not take the influence of domain wall and electrostatic field into account and thus it is not applicable for ferroelectric single crystal with domain configurations. Xiao and co-workers,[19] and Hong *et al.*[20] developed phase field models to study the interactions of oxygen vacancies with domain structures in $BaTiO_3$ single crystal, revealing the existence of depletion layers at the metal-ferroelectric interfaces and vacancy accumulation in 90° domain wall. In these works, the influence of oxygen vacancy was modeled as point charge, and the memory effect and large recoverable electrostrain cannot be captured in the simulations.

Despite the above theoretical studies, several important problems remain and need to be solved. Especially, the interactions of oxygen vacancies with domain evolutions are still not clear, and the mechanism responsible for the memory effect and large recoverable electrostrain is not well understood. A theoretical model that can effectively describe the roles of oxygen vacancies on domain formation is still lacking. In the present study, a two-dimensional ferroelectric model is devised, coupling the classical Ginzburg-Landau theory and the oxygen vacancy diffusion,[19] to demonstrate the influences of oxygen vacancies on domain evolutions under electric field in $BaTiO_3$ single crystal. The oxygen vacancies are modeled as dipoles that possess the symmetry-conforming property[9] and thus can effectively capture the influences of vacancies on domain evolutions. The simulations reproduce well the reversible domain switching and large recoverable electric-field-induced strain observed in experiments with both engineered domain structure[9,10] and

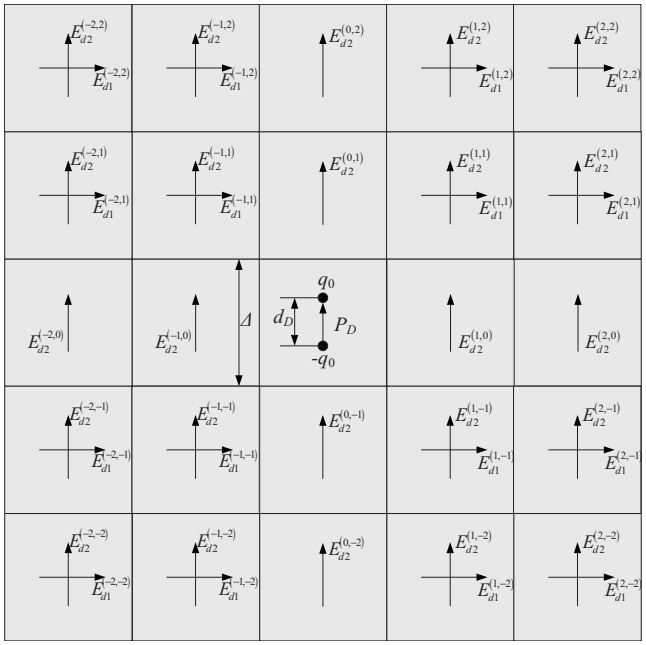

FIG. 1. A two-dimensional model of the defect dipolar field induced by the local defect depolarization. The subscripts of $E_{d1}^{(m,n)}$ and $E_{d2}^{(m,n)}$ denote the components in the x_1 and x_2 directions, and the superscripts mean the induced electric field at the position $(m\Delta, n\Delta)$.

single domain structure.[11] Furthermore, the results indicate that domain memory effect and non-180° domain switching are the mechanisms for large recoverable electrostrain in ferroelectric materials with oxygen vacancies.

II. FORMULATION OF THE PHASE FIELD MODEL

A. Dipolar field induced by oxygen vacancy

Oxygen vacancies and acceptor impurities commonly coexist in ferroelectric lattices, especially after doping.[1,9] Since the oxygen vacancy is in one of the faces of the perovskite cell while the impurity cation is in the center of the cell, they form additional defect dipoles besides the spontaneous ones. Furthermore, the electrons can be localized on the adjacent Ti atom for low vacancy concentrations as we focus on in the study and such electron localization together with the oxygen vacancies can also form defect dipoles. Therefore, it makes more sense to model the influences of oxygen vacancy as defect dipole instead of monopole in this work.[9] Such defect dipole results in additional dipolar electric field in the ferroelectric in addition to the usual depolarization field, through which oxygen vacancies interact with ferroelectric domains and domain walls. In order to describe such interactions, we adopt a continuum model to analyze the oxygen vacancy induced local defect polarization $\mathbf{P}_{defect}$ and the resulted defect dipolar field $\mathbf{E}_{defect}$, and their contribution to the free energy of the ferroelectric system.

To this end, we examine the defect dipole at the atomic scale first. As shown in Fig. 1 for a two-dimensional lattice, the effect of an oxygen vacancy can be modeled as a pair of positive and negative point charges q_0 separated by a distance d_D.[18] The local defect polarization due to the defect dipoles can then be expressed as $P_{defect}=q_0 d_D/\Delta^3$ with Δ denoting the lattice constant of the ferroelectric. The value of d_D has been calculated using first-principles method for $BaTiO_3$ lattice with oxygen vacancy and impurity Fe^{3+} or Cu^{2+}.[21] Based on the electric field distribution induced by point charges, general expressions of the defect dipolar field induced by the local defect polarization at the lattice points $(m\Delta, n\Delta)$ are derived as

$$E_{d1}^{(m,n)} = \frac{P_{defect}}{8\pi B_0 \kappa_0}\left\{\frac{m}{[m^2+(n-B_0)^2]^{3/2}} - \frac{m}{[m^2+(n+B_0)^2]^{3/2}}\right\},$$

$$E_{d2}^{(m,n)} = \frac{P_{defect}}{8\pi B_0 \kappa_0}\left\{\frac{n-B_0}{[m^2+(n-B_0)^2]^{3/2}} - \frac{n+B_0}{[m^2+(n+B_0)^2]^{3/2}}\right\}, \quad (1)$$

where $E_{d1}^{(m,n)}$ and $E_{d2}^{(m,n)}$ denote the two components in the x_1 and x_2 directions, $B_0=d_D/(2\Delta)$ is a constant, and $\kappa_0=8.85\times10^{-12}$ C^2 N^{-1} m^{-2} is the permittivity of the free space. In order to determine the defect dipolar field in the center lattice point shown in Fig. 1, a summation of the contribution from the fifth nearest lattice points is carried out. Such simplification is based on several considerations. First of all, the defect dipolar field decays rapidly by $1/r^3$ as shown by Eq. (1), and a summation of three-dimensional dipoles on a two-dimensional lattice would converge, albeit slowly. Even more importantly, the defect dipole moment decreases quickly away from the 90° domain wall as we demonstrate later, and the dipolar interaction is dominated by localized dipoles near the domain walls. Finally, free charges do exist in $BaTiO_3$ due to its wide band-gap semiconductor characteristics, which can screen the Coulomb long-range interaction. In order to ensure the computational accuracy, we have calculated the relative errors caused by different truncation lengths in the evaluation of the dipolar field. It can be found that using a truncation length of $2\sqrt{2}\Delta$ yields a relative error below 6.8%, which is acceptable in the present model. Therefore, we use a summation of the contribution from the nearest 24 lattice points which form a square of 5×5 unit cells around the center cell, to determine the defect dipolar field in the center lattice point. Due to the antisymmetry of the dipolar field $E_{d1}^{(m,n)}$ about the x_1 axis, the total x_1-directional dipolar field is zero. Noting that the local defect polarization is a vector and using the approximation that $d_D \approx \Delta/2$,[21] a general expression between the local defect polarization and the corresponding defect dipolar field can be derived as

$$E_{i,defect} = \frac{C_0 P_{i,defect}}{\pi \kappa_0}, \quad (2)$$

where C_0 is a constant equal to 1.02.

We then adopt a probability based homogenization method to determine the macroscopic defect polarization. Assuming that the oxygen vacancy density in ferroelectric is N_d, the probability of finding oxygen vacancy in an unit cell can be obtained as $N_d V_0$, where V_0 is the unit cell volume. For a tetragonal $BaTiO_3$ lattice, as shown in Fig. 2, there are six possible oxygen vacancy sites, indexed as (1)–(6). If the

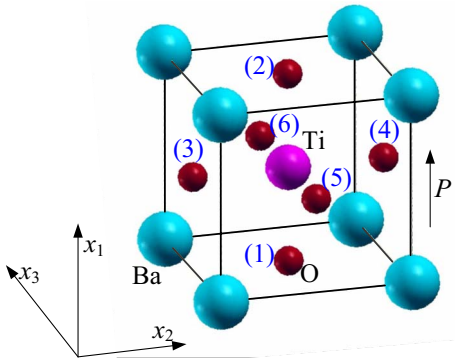

FIG. 2. (Color online) The atomic structure of $BaTiO_3$ unit cell. (1)–(6) are used to index the six oxygen atoms.

polarization is two-dimensional, as consistent with the aforementioned derivation, the possible oxygen vacancy sites are reduced to (1)–(4). Denoting q_i the probability of finding oxygen vacancy at site (i), and using $\mathbf{P}_{(i),o}$ to represent the local defect polarization induced by the oxygen vacancy at site (i), the relation between the macroscopic defect polarization and the oxygen vacancy density can be derived as

$$\mathbf{P}_{defect} = N_d V_0 \sum_{i=1}^{4} q_i \mathbf{P}_{(i),o}. \tag{3}$$

Note that the value of $\mathbf{P}_{(i),o}$ can be calculated by first-principles method, which has been done for $BaTiO_3$ with oxygen vacancy and impurity Fe^{3+} or Cu^{2+}.[21] The probability q_i, which, in general, varies with position, can be determined by minimizing the total free energy of the ferroelectric system with oxygen vacancies. This will be discussed in details in the next section.

B. Energetics of ferroelectrics with oxygen vacancies

In order to investigate the interaction of oxygen vacancies with domains and domain walls in a ferroelectric such as $BaTiO_3$ single crystal, the contributions of vacancy dipolar field to the free energy of the ferroelectric must be considered. To this end, we adopt Landau-Devonshire phenomenological framework with the total energy of the ferroelectric system expressed as

$$G = \int_V [f_{bulk} + f_{grad} + f_{elas} + f_{elec} - \boldsymbol{\sigma}^0 \cdot \boldsymbol{\varepsilon} - \mathbf{E}^0 \cdot \mathbf{P}] dV, \tag{4}$$

where f_{bulk}, f_{grad}, f_{elas}, and f_{elec}, denote the bulk energy density, the gradient energy, the elastic strain energy density, and the electrostatic energy density, respectively, and the last two terms in Eq. (4) represent the potential energies contributed by the external stress $\boldsymbol{\sigma}^0$ and the applied electric field $\mathbf{E}^0$. In the equation, $\boldsymbol{\varepsilon}$ and $\mathbf{P}$ are the transformation strain and spontaneous polarization of the ferroelectric. Notice that the bulk energy density f_{bulk} can be expanded as a polynomial of polarization $\mathbf{P}$ (Ref. 22)

$$\begin{aligned} f_{bulk}(P_i) = {} & \alpha_1(P_1^2 + P_2^2 + P_3^2) + \alpha_{11}(P_1^4 + P_2^4 + P_3^4) + \alpha_{12}(P_1^2 P_2^2 \\ & + P_2^2 P_3^2 + P_1^2 P_3^2) + \alpha_{111}(P_1^6 + P_2^6 + P_3^6) + \alpha_{112}[P_1^2(P_2^4 \\ & + P_3^4) + P_2^2(P_1^4 + P_3^4) + P_3^2(P_1^4 + P_2^4)] + \alpha_{123} P_1^2 P_2^2 P_3^2 \\ & + \alpha_{1111}(P_1^8 + P_2^8 + P_3^8) + \alpha_{1112}[P_1^6(P_2^2 + P_3^2) + P_2^6(P_1^2 \\ & + P_3^2) + P_3^6(P_1^2 + P_2^2)], \end{aligned} \tag{5}$$

where the dielectric stiffness, α_1, varies with temperature while all the other coefficients are constants independent of temperature. The gradient energy penalizes the spatial variation in the order parameter $\mathbf{P}$, and thus is interpreted as the energetic cost of forming domain walls separating different variants

$$\begin{aligned} f_{grad}(P_{i,j}) = {} & \frac{1}{2} G_{11}(P_{1,1}^2 + P_{2,2}^2 + P_{3,3}^2) + G_{12}(P_{1,1}P_{2,2} + P_{2,2}P_{3,3} \\ & + P_{3,3}P_{1,1}) + \frac{1}{2} G_{44}[(P_{1,2}^2 + P_{2,1}^2) + (P_{2,3}^2 + P_{3,2}^2) \\ & + (P_{1,3}^2 + P_{3,1}^2)] + \frac{1}{2} G'_{44}[(P_{1,2}^2 - P_{2,1}^2) + (P_{2,3}^2 \\ & - P_{3,2}^2) + (P_{1,3}^2 - P_{3,1}^2)], \end{aligned} \tag{6}$$

where G_{11}, G_{12}, G_{44}, and G'_{44} are the gradient energy coefficients and the commas in the subscripts denote spatial differentiation. The elastic energy density can be expressed as

$$f_{elas} = \frac{1}{2} c_{ijkl} e_{ij} e_{kl} = \frac{1}{2} c_{ijkl}(\varepsilon_{ij} - \varepsilon_{ij}^0)(\varepsilon_{kl} - \varepsilon_{kl}^0), \tag{7}$$

where e_{ij}, ε_{ij} and ε_{ij}^0 are the elastic strain, the total strain and the transformation strain, respectively, and for a cub-to-tetragonal ferroelectric transformation, the transformation strain $\boldsymbol{\varepsilon}^0$ can be determined from spontaneous polarization $\mathbf{P}$ as following:

$$\begin{aligned} \varepsilon_{11}^0 &= Q_{11}P_1^2 + Q_{12}(P_2^2 + P_3^2), \quad \varepsilon_{13}^0 = Q_{44}P_1P_3, \\ \varepsilon_{22}^0 &= Q_{11}P_2^2 + Q_{12}(P_1^2 + P_3^2), \quad \varepsilon_{23}^0 = Q_{44}P_2P_3, \\ \varepsilon_{33}^0 &= Q_{11}P_3^2 + Q_{12}(P_1^2 + P_1^2), \quad \varepsilon_{12}^0 = Q_{44}P_1P_2, \end{aligned} \tag{8}$$

where Q_{11}, Q_{12}, and Q_{44} are the electrostrictive coefficients. Up to this point, our energetics is identical to the classical Landau-Devonshire phenomenological theory.

For a ferroelectric system with oxygen vacancies, we need to consider not only the electrostatic interactions among spontaneous polarization but also the electrostatic interactions among defect polarizations, and between the spontaneous and defect polarizations. This is where we deviate from the classical theory. In particular, the electrostatic energy in ferroelectric with oxygen vacancy can be expressed as

$$f_{elec} = -\frac{1}{2}(E_{i,p} + E_{i,defect})(P_i + P_{i,defect}), \tag{9}$$

where the electrostatic field $\mathbf{E}_p$ induced by the spontaneous polarization can be further expressed as a negative gradient of the electrostatic potential ϕ, i.e., $E_{i,p} = -\phi_{,i}$, which can be determined by solving the following Maxwell's equation[23,24]

$$\kappa\kappa_0(\phi_{,11}+\phi_{,22}+\phi_{,33})=P_{1,1}+P_{2,2}+P_{3,3}, \tag{10}$$

where κ is the relative permittivity of the ferroelectric. Under typical oxygen vacancy density,[19] on the order of 1×10^{24} m^{-3}, the defect polarization is three orders smaller than the spontaneous polarization as determined from Eq. (3), and thus the electrostatic energy density can be simplified as

$$f_{elec}=-\frac{1}{2}(E_{i,p}+E_{i,defect})P_i. \tag{11}$$

Thus the influence of oxygen vacancy is described by the vacancy dipolar field in this framework. In an equilibrium state with minimum free energy, both the defect polarization $\mathbf{P}_{defect}$ and the corresponding defect dipolar field $\mathbf{E}_{defect}$, should be along the same direction as the spontaneous polarization given sufficient time for relaxation. This implies that the defect dipoles should conform with the direction of spontaneous polarization as postulated by Ren[9] and also confirmed by experimental observations[25] and first-principles calculations.[21] As such, the probabilities q_i can be determined from the spontaneous polarization, and the corresponding defect polarization can be derived as

$$\mathbf{P}_{defect}=N_dV_0P_{defect0}\frac{\mathbf{P}}{|\mathbf{P}|}, \tag{12}$$

where $|\mathbf{P}|$ denotes the magnitude of the spontaneous polarization and $P_{defect0}$ refers to the magnitude of the local defect polarization.

C. Kinetics

The evolutions of the spontaneous polarization and oxygen vacancy distribution are controlled by different kinetics, as described below. The temporal and spatial variations in spontaneous polarizations are governed by the classical time dependent Ginzburg-Landau equation

$$\frac{\partial\mathbf{P}(\mathbf{r},t)}{\partial t}=-L\frac{\delta G}{\delta\mathbf{P}(\mathbf{r},t)}, \tag{13}$$

where $\mathbf{r}$ is the spatial vector, t is the generalized time, and L is the kinetic coefficient. On the other hand, the density of oxygen vacancy is governed by the diffusion equation[19,20]

$$\frac{\partial N_d}{\partial t}=\nabla\cdot\left[\beta N_d\nabla\left(\frac{\partial W_d}{\partial N_d}+ez\phi\right)\right], \tag{14}$$

where β is the mobility and W_d is the contribution to the free energy due to defects, which is assumed to be the usual free energy of mixing at small concentrations, and z represents the donor valency. In the diffusion dynamics, while the impurity atoms can hardly diffuse since their atomic weights are much larger than that of the oxygen atom, the localization of electrons can occur in new adjacent Ti atoms after the diffusion of oxygen vacancies. As such, it is expected that the distribution of defect dipole can vary in accordance with the diffusion of oxygen vacancy. From Eq. (14), it can be found that the polarization evolution and oxygen diffusion are coupled only from the electrostatic potential and thus the electrostatic effect is the main factor that contributes to the diffusion of the oxygen vacancies. Since the variation in oxygen vacancies are governed by diffusion process, it is much slower than the polarization evolution, and the distribution of oxygen vacancies requires substantial longer time to reach the equilibrium.

D. Numerical implementation and simulation parameters

The continuum model has been implemented into numerical simulation on a two-dimensional 64×64 supercell to investigate the interactions between oxygen vacancies and domains and domain walls. To solve the evolution equations numerically, a semi-implicit finite difference scheme is adopted on a time scale,[26,27] and fast Fourier transform is adopted on a spatial scale. Barium titanate is chosen for as a model system in the present simulation and the material constants used in the simulations are listed as following:[22]

$$\alpha_1=4.124\times(T-388)\times10^5\ \ (\mathrm{C^{-2}\,m^2\,N}),$$

$$\alpha_{11}=-209.7\times10^6\ \ (\mathrm{C^{-4}\,m^6\,N}),$$

$$\alpha_{12}=797.4\times10^7\ \ (\mathrm{C^{-4}\,m^6\,N}),$$

$$\alpha_{111}=129.4\times10^7\ \ (\mathrm{C^{-6}\,m^{10}\,N}),$$

$$\alpha_{112}=-195.0\times10^7\ \ (\mathrm{C^{-6}\,m^{10}\,N}),$$

$$\alpha_{123}=-250.0\times10^7\ \ (\mathrm{C^{-6}\,m^{10}\,N}),$$

$$\alpha_{1111}=386.3\times10^8\ \ (\mathrm{C^{-8}\,m^{14}\,N}),$$

$$\alpha_{1112}=252.9\times10^8\ \ (\mathrm{C^{-8}\,m^{14}\,N}),$$

$$\alpha_{1122}=163.7\times10^8\ \ (\mathrm{C^{-8}\,m^{14}\,N}),$$

$$\alpha_{1123}=136.7\times10^8\ \ (\mathrm{C^{-8}\,m^{14}\,N}),$$

$$Q_{11}=0.10\ \ (\mathrm{C^{-1}\,m^2}),$$

$$Q_{12}=-0.034\ \ (\mathrm{C^{-1}\,m^2}),$$

$$Q_{44}=0.029\ \ (\mathrm{C^{-1}\,m^2}).$$

The following normalization of field variables and material parameters are adopted, as described in Ref. 28

$$\mathbf{r}^*=\sqrt{|\alpha_1|/G_{110}}\mathbf{r},\quad t^*=|\alpha_1|Lt,\quad \mathbf{P}^*=\mathbf{P}/P_0,$$

$$\alpha_1^*=\alpha_1/|\alpha_1|,\quad \alpha_{11}^*=\alpha_{11}P_0^2/|\alpha_1|,\quad \alpha_{12}^*=\alpha_{12}P_0^2/|\alpha_1|,$$

$$\alpha_{111}^*=\alpha_{111}P_0^4/|\alpha_1|,\quad \alpha_{112}^*=\alpha_{112}P_0^4/|\alpha_1|,$$

$$\alpha_{123}^*=\alpha_{123}P_0^4/|\alpha_1|,\quad \alpha_{1111}^*=\alpha_{1111}P_0^6/|\alpha_1|,$$

$$\alpha_{1112}^*=\alpha_{1112}P_0^6/|\alpha_1|,\quad \alpha_{1122}^*=\alpha_{1122}P_0^6/|\alpha_1|,$$

TABLE I. The normalized material parameters adopted in the present simulations.

α_1^*	α_{11}^*	α_{12}^*	α_{111}^*	α_{112}^*	α_{123}^*	α_{1111}^*	α_{1112}^*	α_{1122}^*	α_{1123}^*
−1.00	−0.39	1.49	0.16	−0.25	−0.31	0.33	0.22	0.14	0.12
Q_{11}^*	Q_{12}^*	Q_{44}^*	c_{11}^*	c_{12}^*	c_{44}^*	G_{11}^*	G_{12}^*	G_{44}^*	$G_{44}'^*$
0.0068	−0.0023	0.0020	72556	39294	49729	0.6	0.0	0.3	0.3

$$\alpha_{1123}^* = \alpha_{1123} P_0^6 / |\alpha_1|, \quad Q_{11}^* = P_0^2 Q_{11}, \quad Q_{12}^* = P_0^2 Q_{12},$$

$$Q_{44}^* = P_0^2 Q_{44}, \quad c_{11}^* = c_{11}/(|\alpha_1| P_0^2), \quad c_{12}^* = c_{12}/(|\alpha_1| P_0^2),$$

$$c_{44}^* = c_{44}/(|\alpha_1| P_0^2), \quad E^* = E/(|\alpha_1| P_0), \quad \kappa_0^* = \kappa_0 |\alpha_1|,$$

$$G_{11}^* = G_{11}/G_{110}, \quad G_{12}^* = G_{12}/G_{110}, \quad G_{44}^* = G_{44}/G_{110},$$

$$G_{44}'^* = G_{44}'/G_{110}.$$

The Voigt notation is adopted for the elastic stiffness. The reference value of the polarization and the gradient energy are $P_0 = 0.26$ C m^{-2} and $G_{110} = 1 \times 10^{-7}$ C^{-2} m^4 N, respectively. Since the value of α_1 at 300K is $\alpha_0 = -3.63 \times 10^7$ C^{-2} m^4 N, the grid spacing in real space is $l_0 = \sqrt{G_{110}/|\alpha_1|} \approx 52$ nm. The normalized value of the electrostatic potential is calculated by $\phi^* = \phi/\phi_0$, where $\phi_0 = \sqrt{G_{110}|\alpha_0| P_0^2} \approx 0.50$ V. According to the first principle calculations,[21] $P_{defect0} = 0.515$ V m^{-2} is adopted in the simulations. The full list of the normalized material parameters are given in Table I. As the diffusion of oxygen vacancies is usually much slower than evolution of polarizations, the time steps of the polarization and diffusion of defects are set as 0.03 and 0.004,[20] respectively, in order to obtain reasonable and convergent results.

III. SIMULATION RESULTS AND DISCUSSION

In this section, the phase field model developed is employed to study two important issues toward the interactions of oxygen vacancies with domain evolutions: (i) the distribution of defect density in different domain structures and (ii) the influence of oxygen vacancy on the electromechanical responses of different domain structures under an electric field. In the first question, we assume that the ferroelectric is sufficiently aged, such that the time is long enough for the oxygen vacancies to diffuse to the equilibrium state. In the second question, the time scale is small relative to the oxygen vacancy diffusion process, so that only domain switching takes place while oxygen vacancy distribution remains unchanged, away from the equilibrium state. As such, we fix oxygen vacancy distribution and the corresponding defect polarization in this set of simulations.

The interactions of oxygen vacancies with three different domain structures are studied, including a rank-2 domain structure with both 90° and 180° domains,[29,30] a rank-1 domain structure with 180° domains, and a single domain state as described in details in the following sections.

A. Rank-2 domain structure with both 90° and 180° domains

We first consider a rank-2 domain structure with both 90° and 180° domains, as shown in Fig. 3(a), where four ferroelectric variants separated by 90° and 180° domain walls coexist in the ferroelectric. Such domain structure is obtained from phase field simulation without considering the effect of oxygen vacancies and it can be found such domain structure is indeed observed in experiments in $BaTiO_3$ single crystal,[29] as shown in Fig. 3(b).

Using such domain configuration as the initial condition for the polarization distribution, and assuming the oxygen vacancies are uniformly distributed initially with random noises, we solve the evolution equations for the polarization and oxygen vacancies simultaneously, which stabilize after about 1000 simulation steps. The resulting distribution of the electrostatic potential and oxygen vacancy density are shown in Figs. 4(a) and 4(b), respectively. Since there are four different polar domains coexisting, the potential distribution is obviously inhomogeneous. Detailed examination shows that the electric potential changes abruptly at the 90° domain walls but not at the 180° domain walls, consistent with earlier studies.[20] Large depolarization field exists at the 90° domain wall, with the maximum magnitude as high as 5.1MV/m. Such large electric field has also been found in ferroelectrics through the quantum mechanics calculations.[15] The inhomogeneous electrostatic field furthermore drives the redistribution of oxygen vacancies, as shown in Fig. 4(b). It is found that the oxygen vacancies are attracted to different sides of the 90° domain wall but no such accumulation occurs near the 180° domain wall, also consistent with previous studies. This can be used to explain the domain wall pinning and the resulted polarization fatigue. Note that the influence of oxygen vacancy was modeled as point charge in previous studies[20] and the domain memory effect cannot be predicted.[20] In our work, the oxygen vacancies are modeled as dipoles instead.

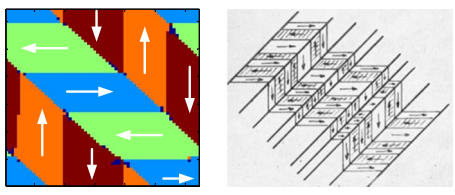

(a) (b)

FIG. 3. (Color online) The engineering domain structures with both 90° and 180° domain walls: (a) calculated by the phase field simulation and (b) observed by experiments in $BaTiO_3$ single crystal (Ref. 29). The arrow represents the polarization direction.

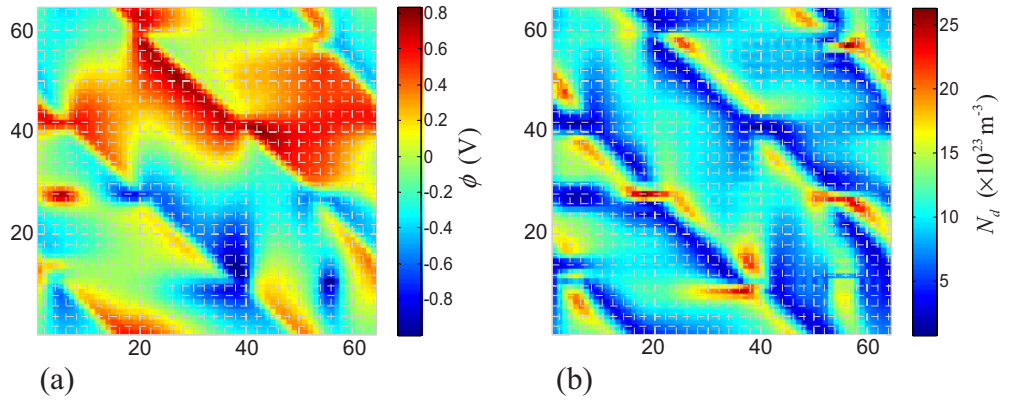

FIG. 4. (Color online) (a) The distributions of electrostatic potential and (b) oxygen vacancy density in the rank-2 domain structure. The initial oxygen vacancy density is uniformly distributed with a magnitude of $N_d = 1 \times 10^{24}$ m^{-3}.

To examine the influences of the oxygen vacancies on the electromechanical responses of the $BaTiO_3$ single crystal, an alternating electric field is applied to pole and depole the material periodically. Due to the symmetry of the polarization distribution, the electromechanical properties are the same in the x_1 and x_2 directions. Notice that the distribution of the oxygen vacancies is fixed in this set of simulations since the diffusion of oxygen vacancies is much slower than domain switching. Three different oxygen vacancy densities are adopted in the simulations and the resulted hysteresis and butterfly loops are shown in Fig. 5. It is found that the electromechanical responses are sensitive to oxygen vacancy density N_d. When N_d is relatively small, i.e., $N_d = 0.5 \times 10^{24}$ m^{-3}, the electromechanical responses are similar to that of the traditional ferroelectric material since the defect dipolar field is not sufficient to switch the domain to the original configuration. When N_d is relatively large, i.e., $N_d = 0.9 \times 10^{24}$ m^{-3} or 1.2×10^{24} m^{-3}, a double hysteresis loop can be found, which indicates that the domain returns to the original configuration after the removal of electric field. Such domain evolution process is indeed observed as shown in Fig. 5(c). Note that the physical origin of the double hysteresis loop is the depolarization field induced by the oxygen vacancy that leads to the recovery of the original domain configuration after the removal of the external electric field. Since a large amount of 90° domain switching occurs during the poling and depoling processes, large recoverable strain induced by the electric field can be found in Fig. 5(b). Fur-

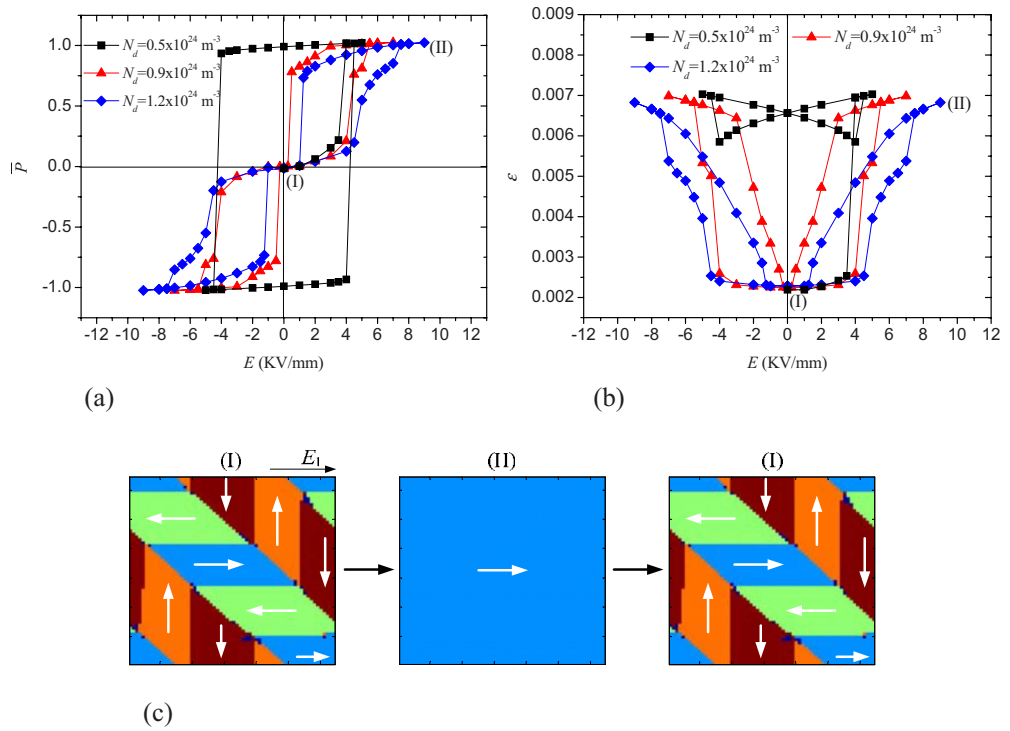

FIG. 5. (Color online) (a) The electric hysteresis loops and (b) butterfly loops of rank-2 domain structures with different oxygen vacancy densities, (c) and the domain evolutions for $N_d = 1.2 \times 10^{24}$ m^{-3} under a positive alternating field. Domains indexed by (i) and (II) in Fig. 5(c) correspond to the two states (i) and (II) in Figs. 5(a) and 5(b).

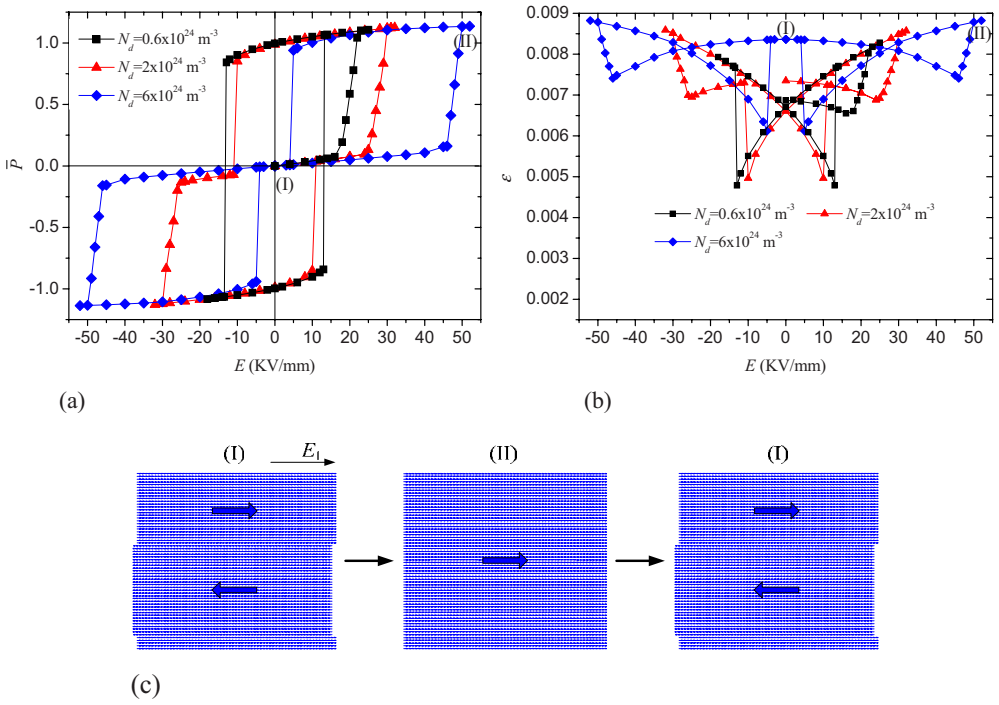

FIG. 6. (Color online) (a) The electric hysteresis loops and (b) butterfly loops of 180° domain structures under an electric loading along the x_1 axis, (c) and the domain evolutions for $N_d=6\times10^{24}$ m^{-3} under a positive alternating field. Domains indexed by (i) and (II) in Fig. 6(c) correspond to the two states (i) and (II) in Figs. 6(a) and 6(b).

thermore, the electric-field-induced strain for $N_d=1.2\times10^{24}$ m^{-3} is about ten times larger than the case of $N_d=0.5\times10^{24}$ m^{-3}. Such double hysteresis loop and large recoverable strain were indeed observed in aged $BaTiO_3$ single crystal.[9,10]

B. 180° domain structure

We then examine ferroelectric crystal with rank-1 domain structure containing 180° domains. There are two ferroelectric variants separated by 180° domain walls, obtained from the phase field simulation for a perfect $BaTiO_3$ single crystal without oxygen vacancy. Using such domain configuration as the initial condition for polarization, and assuming the oxygen vacancies are distributed uniformly with random noises initially, we allow the polarization and oxygen vacancies to evolve simultaneously, which stabilize after about 1000 simulation steps. Since the divergence of polarization is zero in the whole simulation cell, both the electrostatic potential and the oxygen vacancy density are uniformly distributed, even though 180° domain wall exists in the ferroelectric. This is also consistent with the simulation of previous works.[20]

Different from the rank-2 domain structure, the electromechanical properties of the 180° domain structure are distinct in the x_1 and x_2 axes. Therefore, two sets of simulations with the electric field along x_1 and x_2 axes are carried out. The hysteresis and butterfly loops of the ferroelectric under an electric field in the x_1 axis are shown in Fig. 6, and for different oxygen vacancy densities, different characteristics are observed. For $N_d=0.6\times10^{24}$ m^{-3}, 2×10^{24} m^{-3}, and 6×10^{24} m^{-3}, the hysteresis exhibits a typical single-loop, a stepwise-loop, and a double-loop shape, respectively. Such variations in the hysteresis loops with the increase in oxygen vacancies have been also observed in experiments on Nd^{3+}-doped lead strontium zirconate titanate ceramics.[31] On the other hand, it can be found that no large recoverable strain induced by electric field is observed due to the lack of 90° domain switching. This suggests that double hysteresis loop is not a sufficient condition for large recoverable strain induced by electric field.

If the electric field is applied along the x_2 axis instead, the hysteresis and butterfly loops are distinctly different, as shown in Fig. 7. The 180° domain structure all experiences 90° switching after the poling processes for the three oxygen vacancy densities, $N_d=0.3\times10^{24}$ m^{-3}, 0.5×10^{24} m^{-3}, and 0.9×10^{24} m^{-3}. When N_d is relatively small, i.e., $N_d=0.3\times10^{24}$ m^{-3}, the defect dipolar field is not sufficient to switch the domain to the original configuration after further evacuation of applied field. However, when N_d is sufficiently large, i.e., $N_d=0.5\times10^{24}$ m^{-3} or 0.9×10^{24} m^{-3}, the domain memory effect and large recoverable electric-field-induced strain appear in the $BaTiO_3$. They are similar to those observed in rank-2 domain structure since 90° domain switching is involved. Thus even though 180° domain structure does not exhibit domain wall pinning, and there is no accumulation of oxygen vacancy near the domain wall, it still possesses large recoverable electric-field-induced strain in the x_2 direction when N_d is large enough. This conclusion is consistent with the previous experiment results.[11] These two sets of simulations may lead to the conclusion that domain memory effect and non-180° domain switching are the mechanisms for emergence of large recoverable electric-field-induced strain.

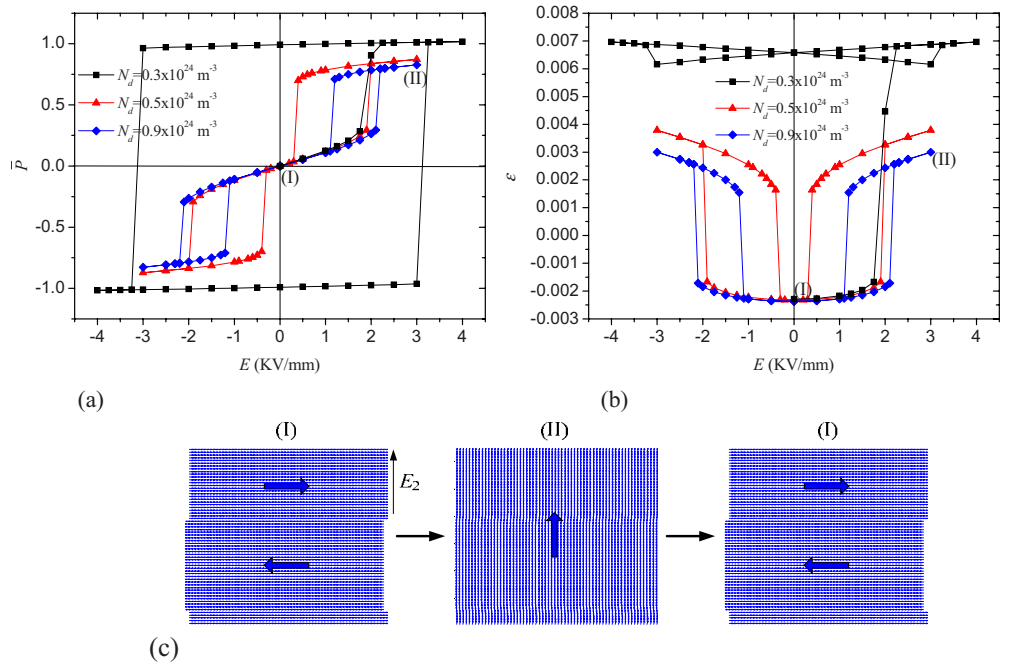

FIG. 7. (Color online) (a) The electric hysteresis loops and (b) butterfly loops of 180° domain structures under an electric loading along the x_2 axis, (c) and the domain evolutions for $N_d=0.9\times10^{24}$ m^{-3} under a positive alternating field. Domains indexed by (i) and (II) in Fig. 7(c) correspond to the two states (i) and (II) in Figs. 7(a) and 7(b).

C. Single domain structure

Finally, we examine a single domain state. Since the divergence of polarization vanishes, both the electrostatic potential and the oxygen vacancy are uniformly distributed after convergence, the same as that of 180° domain structure. Again, two different loading conditions are considered with the electric field applied along x_1 and x_2 axes, respectively. When the electric field is applied along the x_2 axis, the hysteresis and butterfly loops of single domain structure are almost the same as that of 180° domain structure, as shown in Fig. 7. Large recoverable strain can be obtained, which has also been observed in experiments on single domain $BaTiO_3$ single crystal under an electric field perpendicular to the polarization direction.[11] Under an electric field applied in the x_1 axis, the hysteresis and butterfly loops are shown in Fig. 8. Since the defect depolarization field induced by the oxygen vacancy is along the x_1 direction, the hysteresis loops and butterfly loops deviate from the origin of the axis, and the offset becomes larger with the increased oxygen vacancy density. Such asymmetry has been observed in many experiments on ferroelectrics.[5,32] It is also found that the hysteresis and butterfly loops shift to the left of the vertical axis when the oxygen vacancy density is large enough (e.g., $N_d=3.5\times10^{24}$ m^{-3}), indicating that the material exhibits domain memory effect. However, because of no occurrence of non-180° domain switching, there does not appear large recoverable strain as shown in Fig. 8(b). This again demonstrates that domain memory effect is only one necessary condition of large recoverable strain.

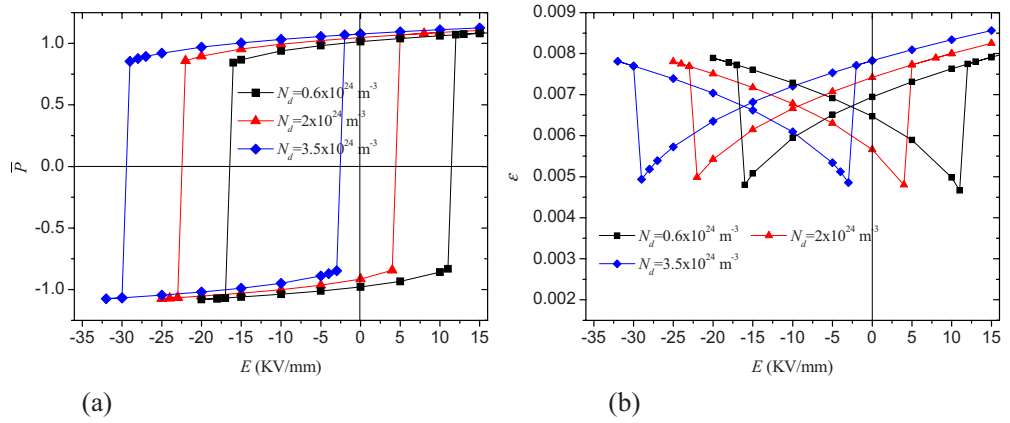

FIG. 8. (Color online) (a) The electric hysteresis loops and (b) butterfly loops of single domain structures under an electric loading along the x_1 axis.

IV. CONCLUSION

In summary, a phase field method has been developed to study the influences of oxygen vacancies on the electromechanical responses of three different domain structures: rank-2 engineered domain structure, 180° domain structure and single domain structure. The oxygen vacancies are modeled as dipoles in this study, which enables the capture of domain memory effect. Furthermore, the simulations reproduce well the reversible domain switching and large recoverable electric-field-induced strain observed in experiments on both engineered domain structure[9,10] and single domain structure.[11] Besides, the following conclusions can be reached: (1) domain memory effect and non-180° domain switching are the mechanisms for large recoverable electric-field-induced strain in ferroelectric materials with oxygen vacancies. (2) Domain wall pinning is not the mechanism for large recoverable electric-field-induced strain. (3) The double hysteresis loop, the stepwise hysteresis loop and shifted hysteresis loop, which have been observed in aged ferroelectric materials,[31,32] are mainly due to the vacancy induced depolarization field.

ACKNOWLEDGMENT

The authors are grateful for the support from Natural Science Foundation of China under Grants No. 10572069, No. 10820101048, and No. 10732100.

*Corresponding author.
†jjli@u.washington.edu
‡fangdn@pku.edu.cn

[1] B. Guiffard, D. Audigier, L. Lebrun, M. Troccaz, and E. Pleska, J. Appl. Phys. **86**, 5747 (1999).
[2] W. Li, A. P. Chen, X. M. Lu, and J. S. Zhu, J. Appl. Phys. **98**, 024109 (2005).
[3] Z. Zhang, L. Lu, C. Shu, and P. Wu, Appl. Phys. Lett. **89**, 152909 (2006).
[4] K. W. Plessner, Proc. Phys. Soc. B **69**, 1261 (1956).
[5] S. Takahashi, Ferroelectrics **41**, 277 (1982).
[6] G. Arlt and H. Neumann, Ferroelectrics **87**, 109 (1988).
[7] C. A. P. de Araujo, J. D. Cuchiaro, L. D. Mcmillan, M. C. Scott, and J. F. Scott, Nature (London) **374**, 627 (1995).
[8] Y. Wang, Q. Y. Shao, and J. M. Liu, Appl. Phys. Lett. **88**, 122902 (2006); Y. Wang, K. F. Wang, C. Zhu, T. Wei, J. S. Zhu, and J. M. Liu, J. Appl. Phys. **101**, 046104 (2007).
[9] X. Ren, Nature Mater. **3**, 91 (2004).
[10] L. X. Zhang and X. Ren, Phys. Rev. B **71**, 174108 (2005); X. Ren and L. X. Zhang, Mater. Sci. Eng., A **438-440**, 1071 (2006); L. X. Zhang and X. Ren, *ibid.* **438-440**, 354 (2006).
[11] L. Zhang and X. Ren, Phys. Rev. B **73**, 094121 (2006).
[12] Z. Feng and X. Ren, Phys. Rev. B **77**, 134115 (2008); Appl. Phys. Lett. **91**, 032904 (2007).
[13] L. He and D. Vanderbilt, Phys. Rev. B **68**, 134103 (2003).
[14] B. Meyer and D. Vanderbilt, Phys. Rev. B **65**, 104111 (2002).
[15] Q. Zhang and W. A. Goddard, Appl. Phys. Lett. **89**, 182903 (2006).
[16] M. Dawber and J. F. Scott, Appl. Phys. Lett. **76**, 1060 (2000); J. F. Scott and M. Dawber, *ibid.* **76**, 3801 (2000).
[17] V. C. Lo, J. Appl. Phys. **92**, 6778 (2002); K. T. Li and V. C. Lo, *ibid.* **97**, 034107 (2005); H. X. Cao, V. C. Lo, and W. W. Y. Chung, *ibid.* **99**, 024103 (2006).
[18] V. C. Lo, W. W. Y. Chung, H. X. Cao, and X. Dai, J. Appl. Phys. **104**, 064105 (2008).
[19] Y. Xiao and K. Bhattacharya, Arch. Ration. Mech. Anal. **189**, 59 (2008); Y. Xiao, V. B. Shenoy, and K. Bhattacharya, Phys. Rev. Lett. **95**, 247603 (2005); Y. Xiao, Ph.D. thesis, Caltech University, 2005.
[20] L. Hong, A. K. Soh, Q. G. Du, and J. Y. Li, Phys. Rev. B **77**, 094104 (2008).
[21] R. A. Eichel, P. Erhart, P. Traskelin, K. Albe, H. Kungl, and M. J. Hoffmann, Phys. Rev. Lett. **100**, 095504 (2008); P. Erhart, R. A. Eichel, P. Traskelin, and K. Albe, Phys. Rev. B **76**, 174116 (2007); P. Erhart and K. Albe, J. Appl. Phys. **102**, 084111 (2007).
[22] Y. L. Li, L. E. Cross, and L. Q. Chen, J. Appl. Phys. **98**, 064101 (2005).
[23] Y. L. Li, S. Y. Hu, Z. K. Liu, and L. Q. Chen, Appl. Phys. Lett. **81**, 427 (2002).
[24] J. Wang and T. Y. Zhang, Phys. Rev. B **73**, 144107 (2006).
[25] L. X. Zhang, E. Erdem, X. Ren, and R. A. Eichel, Appl. Phys. Lett. **93**, 202901 (2008).
[26] L. Q. Chen, Annu. Rev. Mater. Res. **32**, 113 (2002).
[27] Y. L. Li, S. Y. Hu, Z. K. Liu, and L. Q. Chen, Appl. Phys. Lett. **78**, 3878 (2001).
[28] H. L. Hu and L. Q. Chen, Mater. Sci. Eng., A **238**, 182 (1997).
[29] J. A. Hooton and W. J. Merz, Phys. Rev. **98**, 409 (1955).
[30] J. Y. Li and D. Liu, J. Mech. Phys. Solids **52**, 1719 (2004).
[31] Y. J. Yu and R. N. Singh, J. Appl. Phys. **94**, 7250 (2003).
[32] M. Takahashi, Jpn. J. Appl. Phys. **9**, 1236 (1970).